

# Diffusion Model in Latent Space for Medical Image Segmentation Task

Ngoc Huynh Trinh, Hai Toan Nguyen, Son Ba Luong, Quoc Long Tran

*Institute for Artificial Intelligence*

*University of Engineering & Technology (VNU-UET)*

Hanoi, VietNam

huynhntn@vnu.edu.vn, nguyenhaitoan@vnu.edu.vn, luongsonba270@gmail.com, tqlong@vnu.edu.vn

**Abstract**—Medical image segmentation is essential for supporting clinical diagnosis and treatment planning. With growing imaging demands, AI models are increasingly used to improve the accuracy and efficiency of this task. However, traditional approaches often produce a single segmentation mask per input image, limiting the ability to capture uncertainty in the segmentation process. Recent advancements in generative models for image generation present new opportunities to address these limitations by enabling the generation of multiple segmentation masks for each input image. Nevertheless, the computational complexity and performance of these models remain challenging. In this work, we propose MedSegLat-Diff, a novel model for medical image segmentation that integrates a diffusion-based model (DM) with a variational autoencoder (VAE) to decouple perceptual data compression and generation processes. The VAE compresses input data into a low-dimensional latent space, reducing noise and accelerating learning, while the DM performs segmentation more efficiently within this latent representation. Furthermore, we replace the traditional Mean Squared Error (MSE) loss with a weighted Cross-Entropy (WCE) loss in the perceptual mask compression module to enhance the reconstruction of segmentation masks during the encode–decode process, particularly for tiny nodules. This design emulates the collaborative segmentation approach of multiple doctors, offering a more robust and reliable performance compared to previous methods that replicate the segmentation patterns of individual practitioners. We evaluate our model on three datasets: ISIC-2018, CVC-Clinic, and LIDC-IDRI, demonstrating competitive performance while simultaneously providing the ability to generate confidence maps for deeper analysis by experts. Our results show that MedSegLatDiff achieves prominent segmentation performance while offering enhanced interpretability and consistency for clinical applications.

**Index Terms**—diffusion model, variational autoencoder, medical image segmentation, conditional image generation

## I. INTRODUCTION

Medical image segmentation involves partitioning a medical image into meaningful regions, playing a crucial role in diagnosis, surgical planning, and image-guided procedures. Accurate segmentation helps clinicians better interpret images, facilitate comparisons, and monitor changes over time. However, manually labeling segmentation masks is time-consuming and labor-intensive, motivating the development of automated methods. While classical techniques such as binary thresholding and k-means clustering have shown limited effectiveness, recent advances in artificial

intelligence have enabled the widespread use of machine learning and deep learning models, achieving remarkable results. Typically, these AI models are trained on pre-labeled datasets and can automatically segment new images. Most existing approaches adopt a one-to-one strategy, producing a single segmented output per input image [3], [4], [24], [27]. This means generating only one mask per input, effectively replicating the behavior of a single doctor. However, this approach has inherent limitations when applied to complex and ambiguous data, particularly in medical contexts.

Recently, the development of generative models, particularly diffusion-based models (DM) [6], has led to substantial advances in image generation and synthesis, often producing results superior to earlier approaches such as Generative Adversarial Networks (GAN) [20] and Variational AutoEncoder (VAE) [15], which remain among the most widely used methods in recent years. Beyond their success in general image generation, these models open up new possibilities for medical image segmentation through a one-to-many paradigm. Unlike traditional one-to-one approaches, diffusion-based models can generate multiple segmentation masks for a single input, capturing the model’s uncertainty in ambiguous medical data. Several recent studies have adopted this strategy and demonstrated superior performance and robustness compared to conventional methods [8]–[10], [28]. These results indicate that diffusion-based approaches not only enhance segmentation accuracy but also provide richer information to support clinical decision-making, particularly in challenging cases involving ambiguous or subtle anatomical structures. Moreover, we find that the model’s performance can still be further improved in terms of both speed and accuracy.

In this paper, we propose MedSegLatDiff, a medical image segmentation model that follows a novel one-to-many approach based on DM. Our model incorporates a VAE and consists of two stages. The first performs an encoder–decoder operation between input data and latent representation, while the second stage carries out diffusion processes in the latent space to generate a set of segmentation masks for each input image. By imposing conditioning on the random generation process of the diffusion model in the latent space, the model can generate a set of segmentation masks whose variability captures the uncertainty typically

exhibited by a group of doctors. Therefore, our model can simulate the segmentation process of a group of doctors and is well-suited for medical image segmentation tasks. At the same time, the synthesized results from the generated set of segmented images of the model can compete with previous models and confidence map assists doctors in making more in-depth diagnoses. To the best of our knowledge, the main contributions of this paper are as follows:

- Training and incorporating a VAE model to develop a conditional diffusion-based model in latent space, which reduces noise, compresses image size, and improves both training and inference efficiency.
- Utilizing a weighted Cross-Entropy (CE) loss instead of Mean Squared Error (MSE) for tiny segmentation masks in the VAE model, preventing mask neglect or misinterpretation as noise.
- Proposing MedSegLatDiff for medical image segmentation, which simulates the segmentation process of a group of doctors by generating multiple outputs per input image to approximate their variance. Confidence maps derived from these outputs assist experts in performing more thorough and reliable diagnoses.

The remainder of the paper is organized as follows. Section II reviews recent prominent studies on medical image segmentation, generative models, and autoencoder-based approaches. Section III describes the methods and techniques employed in the proposed model. Section IV presents experimental results on three datasets to demonstrate the model’s effectiveness. Finally, Section V concludes the study and outlines potential directions for future research.

## II. RELATED WORK

**Medical Image Segmentation** is the task of assigning a label to each pixel to determine its class membership. This problem has been extensively studied using various AI architectures. Early models following a one-to-one approach include fully convolutional networks [1] and encoder–decoder architectures with skip connections, such as UNet [3] and UNet++ [4], which extend skip connections for improved feature propagation. Traditional CNN-based models, including nnUNet [24] and ResUNet [27], have further demonstrated strong performance in medical image segmentation. In addition, transformer-based architectures, such as SegFormer [21], have been applied for more comprehensive image analysis, and hybrid approaches combining hypernetworks, such as HyperSeg [2], have also been explored.

**Deep Generative Models** are models initially developed for image synthesis tasks. Among them, VAE [15], which rely on probabilistic latent variable modeling, and GAN [20], which learn through adversarial training, laid the foundation. Meanwhile, DM [6], which produce images by gradually adding noise through a Markov chain process, have recently achieved state-of-the-art performance across various tasks, often matching or surpassing the most advanced GAN techniques [5], [7]. By incorporating conditioning into

the generation process, several diffusion-based models have been applied to medical image segmentation. Specifically, EnsembleDiff [8] combines medical images with noisy images using a concatenation operation during denoising, while SegDiff [9] adds (rather than concatenates) the input image after it passes through a convolutional encoder. MedSegDiff [10] and MedSegDiff-v2 [11] further leverage the Feature Frequency Parser to mitigate high-frequency noise and employ the Spectrum-Space Transformer for semantic feature interaction. Furthermore, diffusion models have been integrated with VAEs, as in Stable Diffusion [12], performing forward and reverse processes in latent space to train the denoising model and synthesize new data. This approach has achieved success in image inpainting, class-conditional image synthesis, and other tasks, including text-to-image synthesis, unconditional image generation, and super-resolution [12]–[14]. Inspired by this, we adopt a latent diffusion approach for medical image segmentation, called MedSegLatDiff. Its stochastic sampling allows generation of multiple segmentation outputs per image, capturing variability similar to that of a group of doctors. This makes it well-suited for handling ambiguous and challenging medical data.

## III. METHOD

The proposed model, MedSegLatDiff, integrates a conditional diffusion-based model with a VAE. This section first provides a brief overview of conditional diffusion models for medical image segmentation and a VAE model for encoding and decoding both medical images and segmentation masks. It then focuses on latent diffusion models (LDMs) with conditioning mechanisms operating in latent space for this task.

### A. Segmentation in image pace

Formally, we consider a medical dataset:

$$\mathcal{D} = \{(X^{(i)}, S^{(i)})\}_{i=1}^N, \quad (1)$$

where  $X^{(i)} \in \mathbb{R}^{H \times W \times C}$  denotes the  $i$ -th medical image,  $S^{(i)} \in \mathbb{R}^{H \times W}$  is its corresponding segmentation mask, and  $N$  is the total number of image–mask pairs in the dataset. The main idea when applying DM for segmentation task is to gradually add noise  $\epsilon \sim \mathcal{N}(0, I)$  to a mask  $S$  through a forward process and progressively remove noise from the noisy image via a reverse process. The forward process starts with the original image  $S_0$  sampled from the mask distribution  $p_{\text{mask}}(S)$  and is defined as:

$$q(S_t | S_{t-1}) = \mathcal{N}(S_t; \sqrt{\alpha_t} S_{t-1}, (1 - \alpha_t)I), \quad (2)$$

$S_t$  denotes the latent variable at step  $t$  in the Markov chain, and  $\alpha_t$  is the noise scheduler controlling the noise variance at each step. Over the course of  $T$  steps, the forward process generates progressively noisier images  $(S_1, S_2, \dots, S_T)$ , with  $S_T \sim \mathcal{N}(0, I)$  representing the noisiest image. Given  $S_0$ , a desirable property of this process [6] is that the

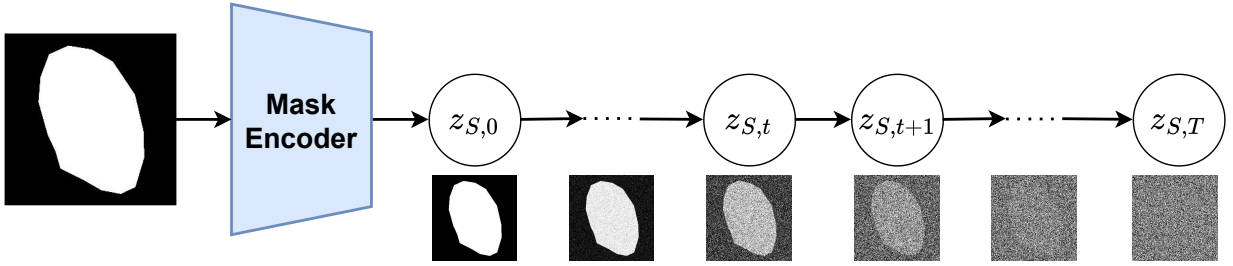


Figure 1. The latent diffusion forward process, where noise is progressively added across diffusion steps.

marginal distribution of  $S_t$  can be obtained by analytically marginalizing out the intermediate latent variables:

$$q(S_t | S_0) = \mathcal{N}(S_t; \sqrt{\gamma_t}S_0, (1 - \gamma_t)I). \quad (3)$$

where  $\gamma_t = \prod_{i=1}^t \alpha_i$ . This forward process generates noisy image pairs that serve as training data for a denoising model  $\epsilon_\theta(S_t, t)$ . The model takes the noisy image  $S_t$  as input and the added noise  $\epsilon$  at step  $t$  as the target. It is trained using a simple Mean Squared Error (MSE) loss:

$$\mathcal{L} = \mathbb{E}_{\epsilon \sim \mathcal{N}(0, I), t} \|\epsilon - \epsilon_\theta(S_t, t)\|_2^2, \quad (4)$$

and is based on a UNet architecture.

For the inference process, we approximate the reverse distribution  $q(S_{t-1} | S_t, S_0)$  by trained denoising model. Therefore, starting from pure Gaussian noise  $S_T \sim \mathcal{N}(0, I)$ , the noise is iteratively reduced at each step to recover  $S_{t-1}$ . This is called as the reverse process and performed as follows:

$$S_{t-1} = \frac{1}{\sqrt{\alpha_t}} \left( S_t - \frac{\sqrt{1 - \alpha_t}}{\sqrt{1 - \gamma_t}} \epsilon_\theta(S_t, t) \right) + \gamma_t \epsilon', \quad (5)$$

where  $\epsilon' \sim \mathcal{N}(0, I)$  introduces stochasticity into the reverse process, and  $t = T, \dots, 1$  denotes the reverse diffusion steps. Therefore, after  $T$  reverse steps, the model can generate multiple segmentation masks  $S_0$ , which approximate samples drawn from the original mask distribution.

However, the setup described above only generates new masks and cannot directly perform segmentation on an input image. Specifically, given a medical image  $X$  and its corresponding segmentation mask  $M$ , an additional channel is appended to the input to incorporate anatomical information. Therefore, the mask and the input image are concatenated channel-wise to obtain

$$S^{\text{cond}} := S \oplus X, \quad (6)$$

where  $\oplus$  denotes channel-wise concatenation. The resulting conditioned representation is then fed into the modified denoising model  $\epsilon(S^{\text{cond}}, t)$ . This concatenation guides the denoising process, ensuring that the model generates new masks corresponding to the input image  $X$ . During the forward process, noise is added only to the ground truth segmentation  $M$ , while  $X$  remains unchanged to preserve anatomical guidance. Since the sampling process is stochastic, the diffusion model generates multiple segmentation

masks  $S_0$  for each input image  $X$ . When trained with a single segmentation mask per image, the model implicitly produces an ensemble of masks, effectively emulating the consensus-driven segmentation process of a group of doctors and potentially improving overall performance.

### B. Image and Mask in latent space

The VAE [15] is a neural network that maps each image from the data distribution to a latent code in a lower-dimensional latent space. It consists of an encoder  $\mathcal{E}(\cdot)$  and a decoder  $\mathcal{D}(\cdot)$ . The encoder maps an image  $X \in \mathbb{R}^{H \times W \times C}$  to a latent representation  $z = \mathcal{E}(X)$ , while the decoder reconstructs the image as  $X' = \mathcal{D}(z) = \mathcal{D}(\mathcal{E}(X))$ , where  $z \in \mathbb{R}^{h \times w \times c}$  lies in a lower-dimensional latent space. The encoder downsamples the image by a factor  $f = \frac{H}{h} = \frac{W}{w}$ , and in our study, we investigate different downsampling factors of the form  $f = 2^m$  with  $m \in \mathbb{N}$ . For our segmentation task, both the medical image  $X$  and the corresponding segmentation mask  $S$  must be transformed into a compact latent space. To achieve this, we employ two separate autoencoders trained independently for images and masks. In particular, we adopt the Vector Quantized Variational Autoencoder (VQ-VAE) [25], [26], whose discrete latent space has demonstrated strong generative performance in recent models such as Stable Diffusion [12]. VQ-VAE is particularly suitable for our setting because: (i) its discrete codebook provides a stable, expressive latent representation; (ii) the quantized latent space is naturally compatible with diffusion models, as demonstrated in Stable Diffusion; and (iii) the stop-gradient mechanism stabilizes training and preserves the piecewise-constant structure characteristic of segmentation masks.

First, we employ a VQ-VAE to encode the input image into a latent space and guide the generation process, ensuring that the predicted mask corresponds to the input image rather than being arbitrary. It consists of an encoder  $\mathcal{E}_X(\cdot)$  that maps the input image  $X$  to a latent representation  $z_X$ , and a decoder  $\mathcal{D}_X(\cdot)$  that reconstructs the image. In addition, a quantization module  $Q_{z_X}(\cdot)$  is designed to discretize the continuous latent representation  $z_X$  into  $\bar{z}_X = Q_{\mathcal{V}_X}(z_X)$  using a codebook  $\mathcal{V}_X = \{v_X^{(k)}\}_{k=1}^K$ . Specifically, each  $d$ -dimensional vector in  $z_X$  is replaced by its nearest codebook entry, and the codebook is jointly learned during training. The optimization objective combines three synergistic terms:

a reconstruction loss to ensure high-fidelity reconstructions

$$\mathcal{L}_{\text{rec}} = \|X - \mathcal{D}_X(\bar{z}_X)\|_2^2, \quad (7)$$

a codebook loss to align encoder outputs with the nearest embeddings

$$\mathcal{L}_{\text{codebook}} = \|\text{sg}(z_X) - \bar{z}_X\|_2^2, \quad (8)$$

and a commitment loss to prevent the encoder outputs from fluctuating excessively

$$\mathcal{L}_{\text{commit}} = \beta \|z_X - \text{sg}(\bar{z}_X)\|_2^2. \quad (9)$$

Here,  $\text{sg}[\cdot]$  denotes the stop-gradient operator, which prevents gradients from flowing into its argument during backpropagation, ensuring that the encoder and the codebook are updated separately. The full objective is then given by

$$\mathcal{L}_{\text{VQ-VAE}} = \mathcal{L}_{\text{rec}} + \mathcal{L}_{\text{codebook}} + \mathcal{L}_{\text{commit}}. \quad (10)$$

Secondly, we design a separate VQ-VAE for the segmentation mask to enable the diffusion-based model to learn the mask distribution in the latent space more efficiently and effectively. It is structured similarly to the image VQ-VAE and consists of an encoder  $\mathcal{E}_S(\cdot)$ , a decoder  $\mathcal{D}_S(\cdot)$ , and a quantization module  $Q_{\mathcal{V}_S}(\cdot)$ , which discretizes the latent representation using a codebook  $\mathcal{V}_S = \{v_S^{(k)}\}_{k=1}^K$ . The key difference lies in our modified loss function, which focuses on the segmented region, with particular emphasis on tiny nodules in the LIDC-IDRI dataset. Instead of using MSE for reconstruction, we adopt WCE to better capture the characteristics of small and sparse lesion regions. The modified reconstruction loss assigns larger weights to pixels within the segmentation mask, enabling the model to focus on these regions and reconstruct the mask more accurately, while all other loss components remain unchanged. This design prevents the perceptual compression model from ignoring tiny nodules, which might otherwise be mistakenly treated as noise.

### C. Segmentation in latent space

Once prepared two pre-trained VQ-VAE models: one for medical images and the other for the corresponding segmentation masks follow by Part III-B, we perform the diffusion processes in the latent domain. For each pair of medical image  $X \in \mathbb{R}^{H \times W \times C}$  and segmentation mask  $S \in \mathbb{R}^{H \times W}$ , the latent data is obtained  $\bar{z}_X$  and  $\bar{z}_S$  corresponding. Using the latent representations, the diffusion model performs the forward diffusion process on each latent mask  $z_{S,0} = \bar{z}_S$ , as illustrated in Fig. 1. This process follows the diffusion mechanism described in Eqs. 2 and 3, which generate noisy labels for the data and train the denoising model.

Similarly, to generate segmentation masks for a medical image  $X$  that are consistent with the input rather than arbitrary, the denoising model incorporates additional conditions derived from the image. These conditions guide the noise removal process and the generation of the corresponding segmentation mask. Specifically, the denoising model takes

as input a combination of the noisy mask  $z_{S,t}$  and the latent image representation  $\bar{z}_X$  as a conditioning signal, using a concatenation operator in the latent space:

$$z_{S,t}^{\text{cond}} = z_{S,t} \oplus \bar{z}_X \quad (11)$$

The denoising model  $\epsilon_\theta(z_{S,t}^{\text{cond}}, t)$  is then trained for the reverse diffusion process. Accordingly, the reverse process in Eq. 5 is modified to incorporate the conditioning as follows:

$$S_{t-1} = \frac{1}{\sqrt{\alpha_t}} \left( S_t - \frac{\sqrt{1-\alpha_t}}{\sqrt{1-\gamma_t}} \epsilon_\theta(z_{S,t}^{\text{cond}}, t) \right) + \gamma_t z \quad (12)$$

Thus, during the inference process, for each latent medical image  $\bar{z}_X$ , a set of  $n$  segmentation masks in the latent space,  $\mathcal{Z}_{S,0} = \{z_S^1, z_S^2, \dots, z_S^n\}$ , is generated from a corresponding set of Gaussian noises,  $\mathcal{Z}_{S,T} = \{z_{S,T}^1, \dots, z_{S,T}^n\}$ . The final step is to map the latent masks back to the original image space using the segmentation mask decoder:

$$S^i = \mathcal{D}_S(z_S^i), \quad (13)$$

where  $i = 1, 2, \dots, n$ . The final output of the model is the set of segmentation masks  $\mathcal{S} = \{S^1, S^2, \dots, S^n\}$ , which can be used to compute a confidence map and generate an implicit ensemble segmentation map. The final consistent result is obtained by averaging the outputs in the set to compute a confidence map, which is then thresholded at 0.5 to produce the final binary segmentation mask. The entire segmentation process is illustrated in Fig. 2. It can fully mimic the segmentation performed by a group of  $n$  doctors, which helps to improve the model's performance.

## IV. EXPERIMENTS

### A. Dataset

We conducted experiments on three datasets. The first dataset, ISIC-2018 [16], was used for the ISIC 2018 Task 1 challenge, which aimed to develop automated binary segmentation of skin lesion areas in dermatoscopic images. The ISIC-2018 dataset was obtained from the official competition website and was collected using web crawling techniques. The second dataset, CVC-Clinic [17], consists of multiple frames extracted from endoscopy videos and is commonly used for medical image segmentation, particularly for polyp detection. This dataset is publicly available on Kaggle, and we accessed it from this platform. The third dataset, LIDC-IDRI [18], contains lesion annotations from experienced thoracic radiologists. Unlike the first two datasets, LIDC-IDRI required specific preprocessing steps. The data was split patient-wise into training, validation, and testing sets in an 8:1:1 ratio. For the LIDC-IDRI dataset, slices containing nodules were extracted from patient cases. The four masks annotated by radiologists were included to evaluate the inter-rater uncertainty between the model's predictions and the expert annotations. For the ISIC-2018 and CVC-Clinic datasets, the default data splits provided by the datasets were used.

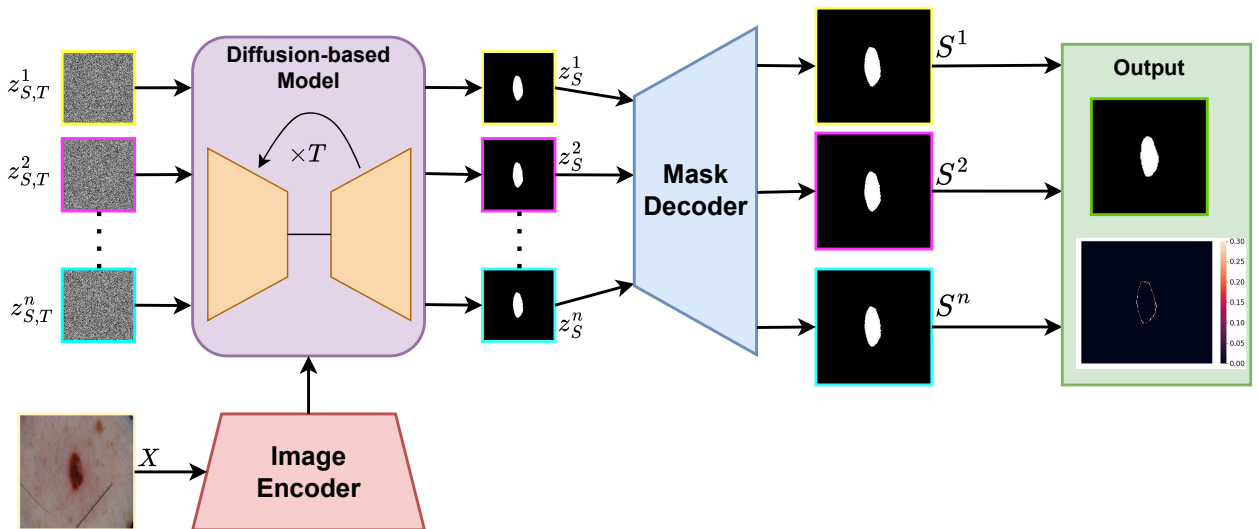


Figure 2. The latent diffusion reverse process, where multiple segmentation masks are generated for a single input medical image.

### B. Implementation Details

We conducted experiments using VQ-VAE for both medical image and mask compression, and a diffusion model (DM) for segmentation in the latent space. The VQ-VAE employs an autoencoder architecture with three downsampling and upsampling layers, while the DM uses a UNet architecture with the same three-level downsampling and upsampling configuration. Both models use 128 base channels. For segmentation mask compression, a Weighted Cross-Entropy (WCE) loss is applied, with a weight of 5 for the positive class. For the LIDC-IDRI dataset, a higher weight of 50 is used due to the small size of the masks. The models are trained for 1000 steps using a simple loss function, following the settings in [6]. All experiments are implemented in PyTorch and conducted on four Tesla V100 GPUs, each with 16 GB of memory. The ISIC-2018 and CVC-Clinic datasets are uniformly resized to 256×256 pixels, while the LIDC-IDRI dataset is resized to 128×128 pixels. The networks are trained end-to-end using the AdamW optimizer [22]. The batch size is set to 32 for the ISIC-2018 and CVC-Clinic datasets and 64 for LIDC-IDRI. The initial learning rate is  $1 \times 10^{-4}$ . During inference, all models utilize 5-fold ensemble predictions to enhance performance. During inference, all models utilize a 5-fold ensemble prediction approach to enhance performance. For a fair comparison, the diffusion-based competitor was also reproduced using the same settings. Additionally, commonly used evaluation metrics, including the Dice coefficient and Intersection over Union (IoU), are employed to quantitatively assess segmentation performance.

### C. Results

We conducted experiments sequentially for two tasks: (1) training a pair of VQ-VAE models for both medical images and masks to map them into the latent space, and (2) training

a conditional diffusion-based model to learn the conditional latent mask distribution in this space. For the first task of perceptual data compression, VQ-VAE demonstrates strong capability in encoding, representing, and reconstructing the data. All results for the VQ-VAE are reported in Table I. For images, we used the default reconstruction loss (MSE). The evaluation metrics were consistently high across all three datasets, achieving an SSIM of 0.94 and PSNR of 34 on both ISIC-2018 and CVC-Clinic. The LIDC-IDRI dataset is more challenging, yielding only 0.89 SSIM and 33.2 PSNR. These results confirm the feasibility of mapping medical images into the latent space using VQ-VAE. For masks, the metrics were extremely high across all four evaluation measures, even when using only MSE loss. Dice and IoU reach 98.4 and 96 on ISIC-2018, while CVC-Clinic performs even better, with Dice and IoU exceeding 99. Although learning binary masks is generally an easier task, LIDC-IDRI produces slightly lower scores because its tiny masks can cause the model to overlook small structures. When switching to Weighted Cross-Entropy (WCE), performance improves across all three datasets. The gains on ISIC-2018 and CVC-Clinic are modest, but LIDC-IDRI benefits substantially, with Dice increasing from 88 to 94.4, IoU from 83.1 to 89.4, and SSIM and PSNR rising by 0.07 and 6.5, respectively. These results demonstrate the adjusted model’s capability to effectively map mask data into the latent space.

For the second task, we provide qualitative results in Fig. 3 across the three datasets. We select five samples and compute their average to generate a confidence map, while using a threshold of 0.5 to visualize the ensemble mask consistency for all cases. For the quantitative analysis, we first examine how the evaluation metrics change as we increase the number of sampling steps, which can be interpreted as increasing the number of experts that the model imitates in a clinical setting. The Dice results are shown in Fig. 4. From 1 to 5

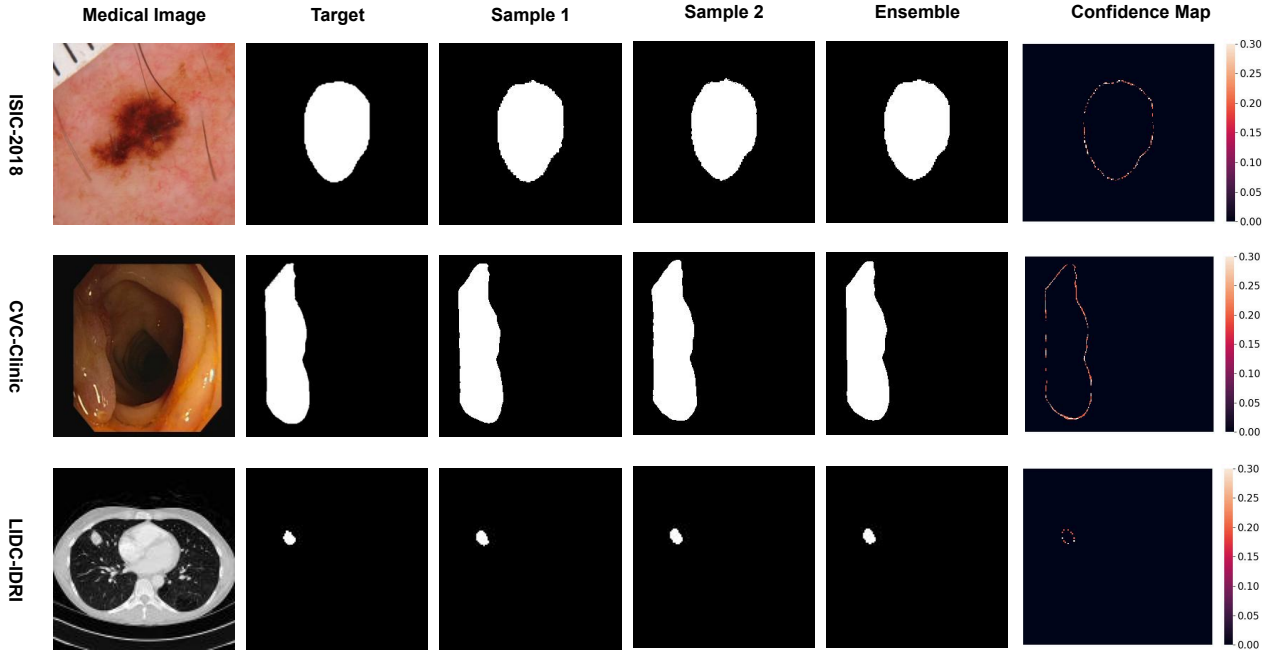


Figure 3. Illustration of our pipeline: two initial mask samples, their averaged output, and the confidence map.

Table I  
PERFORMANCE OF VQ-VAE FOR PERCEPTUAL DATA COMPRESSION.

Dataset	Input (loss)	Dice	IoU	SSIM	PSNR
ISIC-2018	Mask (MSE)	98.0	96.5	0.97.5	38.0
	Mask (WCE)	98.4	96.9	0.98	38.4
	Image (MSE)	-	-	0.94	34.2
CVC-Clinic	Mask (MSE)	99.0	89.9	0.97.6	38.0
	Mask (WCE)	99.5	99.0	0.98	38.7
	Image (MSE)	-	-	0.94	34.5
LIDC-IDRI	Mask (MSE)	88.0	83.1	0.92	35.2
	Mask (WCE)	94.4	89.4	0.99	41.7
	Image (MSE)	-	-	0.90	32.2

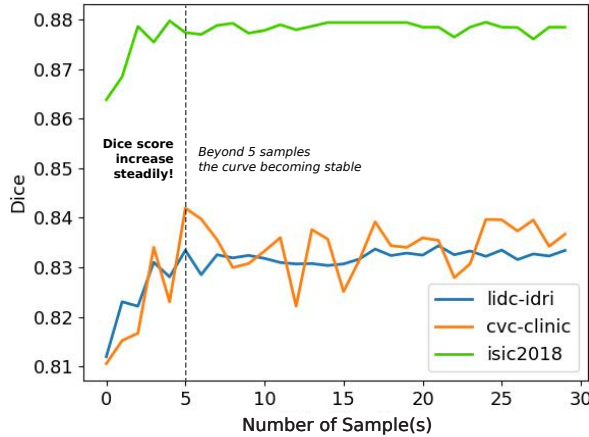


Figure 4. Dice results as the number of sampling steps increase.

samples, the Dice score increases steadily, reflecting clear gains when generating more candidate masks. Specifically,

ISIC-2018 improves from 0.865 to 0.880, CVC-Clinic from 0.81 to 0.845, and LIDC-IDRI from 0.834 to higher values. This trend is expected, as aggregating predictions from more experts typically produces better consensus. Beyond 5 samples, further increasing the number up to 30 yields only marginal benefits, with the curve becoming stable. Based on this observation, we choose 5 samples as the optimal setting, achieving a balance between computational efficiency and segmentation accuracy.

Table II  
COMPARISON OF MEDSEGLatDIFF WITH PREVIOUS ONE-TO-ONE SEGMENTATION MODELS.

Model	ISIC-2018		CVC-Clinic		LIDC-IDRI	
	Dice	IoU	Dice	IoU	Dice	IoU
UNet [3]	85.6	78.5	82.3	72.5	81.0	70.0
UNet++ [4]	81.0	72.9	79.4	70.9	79.9	68.9
ResUNet [27]	87.1	78.2	81.5	71.6	82.1	70.6
nnUNet [24]	87.5	79.5	81.3	71.3	82.8	71.0
MedSegLatDiff	<b>88.0</b>	<b>80.5</b>	<b>84.5</b>	<b>73.1</b>	<b>83.4</b>	<b>71.8</b>

Furthermore, we compared our model against baseline methods, covering both the traditional one-to-one approach and the newer one-to-many paradigm. First, Tab. II presents the results of models following the former approach. Common baselines such as UNet and UNet++ achieved relatively modest performance, whereas ResUNet and nnUNet demonstrated stronger capabilities, reaching around 87 Dice and 79 IoU on ISIC-2018, 82 Dice and 72 IoU on CVC-Clinic, and 82 Dice and 81 IoU on LIDC-IDRI. In contrast, our proposed

Table III  
COMPARISON OF MEDSEGLATDIFF WITH RECENT ONE-TO-MANY SEGMENTATION MODELS.

Model	ISIC-2018		CVC-Clinic		LIDC-IDRI	
	Dice	IoU	Dice	IoU	Dice	IoU
EnsembleDiff [8]	86.6	79.5	83.5	71.9	81.7	70.5
SegDiff [9]	85.3	78.7	82.1	70.1	81.0	70.0
MedSegDiff [10]	<b>88.1</b>	<b>80.5</b>	84.0	72.5	82.5	71.1
MedSegLatDiff	88.0	<b>80.5</b>	<b>84.5</b>	<b>73.1</b>	<b>83.4</b>	<b>71.8</b>

model proves to be the most prominent, achieving superior Dice scores of 88, 84.5, and 83.4 (improvements ranging from 0.5 to 2.0) and IoU scores of 80.5, 73.1, and 71.8 (gains of approximately 0.8 to 1.8) across the three datasets. This highlights the effectiveness of our method over traditional one-to-one segmentation models.

Compared with recent approaches, as shown in Tab. III, our proposed model outperforms all three baselines. EnsembleDiff and SegDiff show less stable performance than MedSegLatDiff. On ISIC-2018, MedSegDiff is slightly competitive with our method, achieving a Dice of 88.1 compared with our 88.0 and the same IoU of 80.5. However, on the other two datasets, our model clearly surpasses all baselines, reaching the best Dice of 84.5 (+0.5) and IoU of 73.1 (+0.6) on CVC-Clinic. A similar trend is observed on the more challenging LIDC-IDRI dataset with tiny masks, where our model achieves a margin of +0.9 Dice and +0.7 IoU over MedSegDiff. Overall, the findings highlight the clear superiority of our proposed model, which achieves the most robust and accurate segmentation results across all benchmarks.

## V. CONCLUSION

In this paper, we proposed MedSegLatDiff, a conditional diffusion model operating in the latent space via VQ-VAE for medical image segmentation. We designed two VQ-VAE modules for images and masks to encode data into a compact latent representation. For perceptual mask compression, incorporating weighted cross-entropy as the reconstruction loss significantly improved the encoding–decoding quality. Our experiments show that using five samples yields stable and reliable results, enabling MedSegLatDiff to outperform previous one-to-one segmentation methods and compete effectively with recent one-to-many approaches. This strategy provides an efficient solution that improves both training and sampling efficiency, thereby enhancing segmentation performance through a sampling process that mimics a group of experts. For future work, we plan to explore more advanced conditioning mechanisms, such as classifier guidance [5], classifier-free guidance [23], and flow-based generative modeling, to further improve stability, calibration, and uncertainty estimation of the model’s outputs.

## ACKNOWLEDGMENT

The computing resources used in this research were sponsored by Intelligent Integration Co., Ltd. (INT2), Vietnam.

## REFERENCES

- [1] J. Long, E. Shelhamer, and T. Darrell, “Fully convolutional networks for semantic segmentation,” in *Proc. IEEE Conf. Comput. Vis. Pattern Recognit.*, 2015, pp. 3431–3440.
- [2] Y. Nirkin, L. Wolf, and T. Hassner, “HyperSeg: Patch-wise hypernetwork for real-time semantic segmentation,” in *Proc. IEEE/CVF Conf. Comput. Vis. Pattern Recognit.*, 2021, pp. 4061–4070.
- [3] O. Ronneberger, P. Fischer, and T. Brox, “U-Net: Convolutional networks for biomedical image segmentation,” in *Medical Image Computing and Computer-Assisted Intervention – MICCAI 2015*, 2015, pp. 234–241.
- [4] Z. Zhou, M. Rahman Siddiquee, N. Tajbakhsh, and J. Liang, “UNet++: A nested U-Net architecture for medical image segmentation,” in *Deep Learning in Medical Image Analysis and Multimodal Learning for Clinical Decision Support*, 2018, pp. 3–11.
- [5] P. Dhariwal and A. Nichol, “Diffusion models beat GANs on image synthesis,” *Adv. Neural Inf. Process. Syst.*, vol. 34, pp. 8780–8794, 2021.
- [6] J. Ho, A. Jain, and P. Abbeel, “Denoising diffusion probabilistic models,” *Adv. Neural Inf. Process. Syst.*, vol. 33, pp. 6840–6851, 2020.
- [7] A. Q. Nichol and P. Dhariwal, “Improved denoising diffusion probabilistic models,” in *Int. Conf. Mach. Learn.*, 2021, pp. 8162–8171.
- [8] J. Wolleb, R. Sandkühler, F. Bieder, P. Valmaggia, and P. C. Cattin, “Diffusion models for implicit image segmentation ensembles,” in *Int. Conf. Medical Imaging with Deep Learning*, 2022, pp. 1336–1348.
- [9] T. Amit, T. Shaharabany, E. Nachmani, and L. Wolf, “SegDiff: Image segmentation with diffusion probabilistic models,” 2021, arXiv:2112.00390.
- [10] J. Wu *et al.*, “MedSegDiff: Medical image segmentation with diffusion probabilistic model,” in *Medical Imaging with Deep Learning*, 2024, pp. 1623–1639.
- [11] J. Wu *et al.*, “MedSegDiff-V2: Diffusion-based medical image segmentation with transformer,” in *Proc. AAAI Conf. Artif. Intell.*, vol. 38, no. 6, pp. 6030–6038, 2024.
- [12] R. Rombach, A. Blattmann, D. Lorenz, P. Esser, and B. Ommer, “High-resolution image synthesis with latent diffusion models,” in *Proc. IEEE/CVF Conf. Comput. Vis. Pattern Recognit.*, 2022, pp. 10684–10695.
- [13] W. H. L. Pinaya *et al.*, “Brain imaging generation with latent diffusion models,” in *MICCAI Workshop on Deep Generative Models*, 2022, pp. 117–126.
- [14] A. Blattmann *et al.*, “Align your latents: High-resolution video synthesis with latent diffusion models,” in *Proc. IEEE/CVF Conf. Comput. Vis. Pattern Recognit.*, 2023, pp. 22563–22575.
- [15] D. P. Kingma and M. Welling, “Auto-encoding variational Bayes,” 2013, arXiv:1312.6114.
- [16] N. Codella *et al.*, “Skin lesion analysis toward melanoma detection 2018: A challenge hosted by the international skin imaging collaboration (ISIC),” 2019, arXiv:1902.03368.
- [17] D. Jha *et al.*, “Kvasir-Seg: A segmented polyp dataset,” in *MultiMedia Modeling*, 2020, pp. 451–462.
- [18] S. G. Armato III *et al.*, “The lung image database consortium (LIDC) and image database resource initiative (IDRI): A completed reference database of lung nodules on CT scans,” *Med. Phys.*, vol. 38, no. 2, pp. 915–931, 2011.
- [19] J. Song, C. Meng, and S. Ermon, “Denoising diffusion implicit models,” 2020, arXiv:2010.02502.
- [20] I. Goodfellow *et al.*, “Generative adversarial networks,” *Commun. ACM*, vol. 63, no. 11, pp. 139–144, 2020.
- [21] E. Xie *et al.*, “SegFormer: Simple and efficient design for semantic segmentation with transformers,” *Adv. Neural Inf. Process. Syst.*, vol. 34, pp. 12077–12090, 2021.
- [22] I. Loshchilov and F. Hutter, “Decoupled weight decay regularization,” 2017, arXiv:1711.05101.
- [23] J. Ho and T. Salimans, “Classifier-free diffusion guidance,” 2022, arXiv:2207.12598.
- [24] F. Isensee *et al.*, “nnU-Net: A self-configuring method for deep learning-based biomedical image segmentation,” *Nat. Methods*, vol. 18, no. 2, pp. 203–211, 2021.
- [25] A. Razavi, A. van den Oord, and O. Vinyals, “Generating diverse high-fidelity images with VQ-VAE-2,” *Adv. Neural Inf. Process. Syst.*, vol. 32, 2019.

- [26] J. Peng, D. Liu, S. Xu, and H. Li, "Generating diverse structure for image inpainting with hierarchical VQ-VAE," in *Proc. IEEE/CVF Conf. Comput. Vis. Pattern Recognit.*, 2021, pp. 10775–10784.
- [27] F. I. Diakogiannis, F. Waldner, P. Caccetta, and C. Wu, "ResUNet-a: A deep learning framework for semantic segmentation of remotely sensed data," *ISPRS J. Photogramm. Remote Sens.*, vol. 162, pp. 94–114, 2020.
- [28] V. P. Nguyen *et al.*, "Aleatoric uncertainty medical image segmentation estimation via flow matching," in *International Workshop on Uncertainty for Safe Utilization of Machine Learning in Medical Imaging*, 2025, pp. 134–144.